Available online at www.sciencedirect.com
SCIENCE DIRECT®
International Journal of Solids and Structures 42 (2005) 4673–4694
INTERNATIONAL JOURNAL OF SOLIDS and STRUCTURES
www.elsevier.com/locate/ijsolstr

Evaluation of atmospheric corrosion damage to steel space structures in coastal areas

B. Chen [a], Y.L. Xu [a,*], W.L. Qu [b]

[a] Department of Civil and Structural Engineering, The Hong Kong Polytechnic University, Hung Hom, Kowloon, Hong Kong
[b] College of Civil Engineering and Architecture, Wuhan University of Technology, Wuhan, China

Received 11 August 2004; received in revised form 8 February 2005
Available online 21 March 2005

Abstract

Steel space structures in coastal areas, often exposed in the open air, are inevitably subjected to atmospheric corrosion. This paper presents a framework for evaluation of potential damage due to atmospheric corrosion to steel space structures in coastal areas through an integration of knowledge in material science and structural analysis. An empirical model for estimating corrosion of steel material is first presented based on long-term experimental data available. Equations relating structural natural frequency sensitivity to structural member thickness are then derived in consideration of both inner and outer surface corrosions of the structural member. The nonlinear static analysis is finally conducted to evaluate effects of atmospheric corrosion on the stress of structural members and the safety of steel space structures. By taking a real large steel space structure built in southern coastal area in China as example, the feasibility of the proposed approach is examined and the potential damage caused by atmospheric corrosion to the structure is assessed. The results demonstrate that the atmospheric corrosion does not obviously affect the natural frequencies of the structure but it does create stress redistribution and some of the structural members may have large stress changes.

Keywords: Steel space structure; Atmospheric corrosion; Sensitivity analysis; Stress redistribution; Damage evaluation

1. Introduction

Engineering steel material can be converted to more stable mineral compounds when exposed to atmospheric environment for certain periods. This action, which is called atmospheric corrosion (Shreir et al.,

* Corresponding author. Tel.: +852 27666050; fax: +852 23346389.
E-mail address: ceylxu@polyu.edu.hk (Y.L. Xu).

0020-7683/$ - see front matter © 2005 Elsevier Ltd. All rights reserved.
doi:10.1016/j.ijsolstr.2005.02.004

1994), can change the chemical and physical properties of the steel and weaken the strength of steel members in an engineering structure. The degradation of steel material due to atmospheric corrosion is of importance for the durability of the structure as a whole and may lead to structural damage accumulation and collapse eventually. Nowadays, large steel engineering structures are widely built throughout the world such as bridges, gymnasiums, exhibition centers, and truss towers to provide special services and functions. However, often exposed in the open air, they are inevitably subjected to atmospheric corrosion. If the accumulating damage cannot be timely detected, the structural safety will be threatened and the damage may finally cause the partial or whole collapse of the structure, resulting in economic lose and faculty casualty (Christofer et al., 2000).

The past four decades witness the rapid development of atmospheric corrosion research in the field of material science with many field measurements and corrosion evaluation methods being proposed (Kucera et al., 1986; Shastry et al., 1988). For instance, the Chinese Science and Technology Committee and the National Natural Scientific Foundation of China have established a national experimental network for atmospheric corrosion of metal materials since 1983, and a huge amount of data have been collected since then. Similar activities have also been carried out in other parts of the world. Based on the data collected in the field, several empirical models have been put forward to predict the atmospheric corrosion of metal materials (Cole, 1994; Farrow and Graedel, 1996; Juan et al., 2003; Hou and Liang, 2004).

International concern has also increased over the past decade as it has become evident that atmospheric corrosion has resulted in substantial deterioration of buildings and structures (Cowell and Apsimon, 1996; Ninomiya et al., 1997). Ibrahim et al. (1994) investigated the atmospheric corrosion of reinforcing steel and its influence on steel weight loss, strength, elongation and bending ability. Batis and Rakanta (2004) examined the performance of four different sets of reinforcing steel bars exposed to the Greek atmosphere before their installation into the concrete. Herrera et al. (1995) conducted an investigation on collapse of a 10 m high steel post caused by atmospheric corrosion in USA. Flavio and Stefano (2002) carried out an extensive failure analysis trying to find the reasons of the early failures of weathering steel used for many years for steel construction in the field of transportation.

A little work has yet been carried out to evaluate effects of atmospheric corrosion on structural behavior and safety of large steel space structures built in coastal areas. This paper first introduces the refined exponential model for estimating corrosion of steel materials at a site using a pattern recognition technique to determine the key parameters in the model. The formulae for relating structural natural frequency sensitivity to structural member thickness are then derived to assess the sensitivity of natural frequency to variation of member thickness due to corrosion. The nonlinear static structural analysis is finally conducted to evaluate effects of atmospheric corrosion on the stress of structural members and the safety of steel space structures. A large steel space structure to be built in southern coastal area of China is taken as the case study to examine the feasibility of the proposed approach and to assess the potential damage caused by atmospheric corrosion to the structure.

2. Empirical model for predicting atmospheric corrosion of metal materials

The study up to now indicates that there are many factors affecting the atmospheric corrosion depth of metal materials. One of the widely used empirical models for predicting atmospheric corrosion depth of metal materials is the exponential model (Feliu and Morcillo, 1993).

$$D = AT^n \tag{1}$$

where D is the corrosion depth in μm; T is the time in year; A and n are the model parameters depending on the type of metal and environmental parameters. Clearly, if the time T equals 1, the corrosion depth D equals A, indicating that the parameter A represents the corrosion depth of the material in the first year.

The first-year atmospheric corrosion A is an important parameter that can be estimated based on commonly available meteorological and pollution data. After having analyzed the extensive atmospheric corrosion data collected from the seven designated locations within the national experimental network in China, Wang et al. (1995) proposed the following logarithmic equation to estimate the parameter A:

$$A = C_1 \log N + C_2 \tag{2}$$

where the coefficients C_1 and C_2 are the constants depending on the type of metal only; and N is the environmental index expressed as

$$N = f_1 + f_2 + f_3 \tag{3}$$

in which f_1, f_2 and f_3 are termed the humidity coefficient, air contamination coefficient, and rain acidity coefficient, respectively. These coefficients are expressed as

$$f_1 = \frac{\text{hours per year for relative humidity} > 80\%}{\text{average temperature per year } (^\circ\text{C}) \times \text{hours with sunshine per year}} \tag{4}$$

$$f_2 = (2[SO_2] + 2[Cl^-] + [NO_2])^{1/2} \tag{5}$$

$$f_3 = \frac{1}{2}\left(\frac{1}{10}\log\frac{\text{precipitation per year (mm/a)}}{\text{days with precipitation per year}}\right)^{|7-\text{pH}|/23} \tag{6}$$

As a result, substituting Eq. (2) into Eq. (1) yields an empirical model for predicting the atmospheric corrosion depth in terms of the type of metal and the environmental index.

$$D = (C_1 \log N + C_2)T^n \tag{7}$$

By applying the regressive analysis to the test data collected from the national experimental network in China, the environmental index N and the corrosion development trend n in Eq. (7) have been estimated for seven cities (see Tables 1 and 2) (Hou et al., 1994; Liang and Hou, 1998), and the constants C_1 and C_2 have also been provided for different types of metal materials (Table 3) (Wang et al., 1995). However, if a steel space structure is located at a city, such as Shenzhen, that is not in the national experimental network, an appropriate way should be found to estimate its environmental index N and the corrosion development trend n. To this end, a pattern recognition technique is used in this study. The nine important environmental parameters in Eqs. (4)–(6) are first normalized for each city using the following equation:

$$x_j = \frac{(x'_j - x'_{j\min})}{(x'_{j\max} - x'_{j\min})} \tag{8}$$

Table 1
Environmental parameters and index N

	Item/site	Shenzhen	Beijing	Qingdao	Wuhan	Jiangjin	Guangzhou	Wanning	Qionghai
x_1	Cl^- deposition (mg/100 cm^2 d)	0.037	0.049	0.250	0.011	0.006	0.024	0.387	0.199
x_2	SO_2 deposition (mg/100 cm^2 d)	0.118	0.442	0.704	0.272	0.667	0.107	0.060	0.150
x_3	NO_2 content (mg/m^3)	0.043	0.220	0.038	0.089	0.007	0.035	0.005	0.008
x_4	Average temperature (°C)	22.1	11.9	12.3	16.8	17.9	22.9	24.2	24.3
x_5	Hours for relative humidity > 80% (h/a)	4730	2558	4049	4181	5741	4700	6020	6241
x_6	Precipitation (mm/a)	1908	586	562	1140	1203	1563	1515	1794
x_7	Precipitation days (days/a)	144	78	94	116	134	170	124	151
x_8	PH	4.7	5.5	6.1	6.5	4.4	5.8	5.0	6.9
x_9	Sunshine hours (h/a)	1822	2559	2161	1621	1317	1607	2026	2072
N	Index	1.113	1.607	2.001	1.438	1.790	1.115	1.483	1.459

Table 2
Corrosion development trend n for different types of metal material in China (Hou et al., 1994)

Type	Beijing	Qingdao	Wuhan	Jiangjin	Guangzhou	Wanning	Qionghai
D36	0.37	0.55	0.31	0.46	0.51	0.64	0.90
16MnQ	0.36	0.51	0.43	0.49	0.64	0.59	0.93
12CrMnCu	0.33	0.38	0.36	0.52	0.55	0.76	0.73
3C	0.35	0.51	0.60	0.47	0.49	1.06	0.66
09MnNb	0.50	0.49	0.41	0.43	0.53	1.04	0.88
A3	0.35	0.44	0.42	0.45	0.45	1.10	0.66
20	0.27	0.52	0.30	0.47	0.47	1.14	0.74
16Mn	0.36	0.54	0.56	0.42	0.48	1.37	0.94
08Al	0.42	0.56	0.69	0.59	0.61	1.97	1.50

Table 3
Coefficients C_1 and C_2 for different types of metal material in China (Wang et al., 1995)

Material	C_1	C_2
D36	34.85	50.16
16MnQ	33.88	51.88
12CrMnCu	36.24	51.40
3C	35.86	52.00
09MnNb	35.11	68.95
A3	39.36	61.34
20	42.09	74.97
16Mn	39.55	65.94
08Al	44.60	176.55

in which x'_j is the value of the jth environmental parameter in a city ($j = 1, 2, \ldots, 9$ in this study); and $x'_{j\min}$ and $x'_{j\max}$ are the minimum and maximum values of the jth environmental parameter among all the cities concerned, including one with unknown N and n.

The matching degree, MD, of the city with unknown N and n to a city with known N and n can then be calculated using the following equation:

$$\mathrm{MD}(Y,Z) = 1 - \sum_{j=1}^{m} \mathrm{abs}[x_j(Y) - x_j(Z)]/m \tag{9}$$

in which MD is the matching degree; Y indicates the city with unknown N and n; Z refers to the city with known N and n; and m is the number of environmental parameters concerned and it is equal to 9 in this study. If there are seven cities with known N and n, seven values of MD can be calculated. The smallest value of MD then indicates that the environmental index N and the corrosion development trend n of the relevant city Z can be used for the city Y. The aforementioned way makes it possible to estimate the environmental index and the corrosion development trend for the city Y through several cities with known N and n.

3. Sensitivity of natural frequency to atmospheric corrosion

A steel space structure, when exposed to natural environment under sun, rain, wind and others, is inevitably affected by atmospheric corrosion, which may result in the loss of section area of its structural members. Most of steel space structures are made of steel members with hollow section. The proper painting of

the outer surface of a structural member can enhance the atmospheric corrosion resistance, but this measure can hardly be used to handle the inter surface of the structural member. The loss of cross section area or the reduction of thickness of the structural member will eventually affect the structural integrity and safety. Thus, it is necessary to put forward some ways to detect the accumulation damage due to atmospheric corrosion to a steel space structure. Since most measurable dynamic characteristic of a steel space structure is its natural frequency, the sensitivity of natural frequency to structural member thickness of a steel space structure and the relationship between the change in natural frequency and the reduction in member thickness are pursued in this study.

Suppose that a finite element model is established for a steel space structure. The matrix eigenvalue problem of the steel space structure can be written as

$$(\mathbf{K} - \omega^2 \mathbf{M})\boldsymbol{\varphi} = 0 \tag{10}$$

where $\mathbf{M}$, $\mathbf{K}$ and $\boldsymbol{\varphi}$ are the mass matrix, stiffness matrix and modal vector of the structure respectively. The mass matrix, stiffness matrix, and modal vector are the function of geometric properties of structural members, such as the thickness t_i of the ith structural member. In a similar way to eigenvalues and eigenvectors in structural sensitivity analysis (Fox and Kapoor, 1968; Mottershead and Friswell, 1993), the first derivative of Eq. (10) to the thickness t_i of the ith structural member for the rth mode vibration results in

$$\left(\frac{\partial \mathbf{K}}{\partial t_i} - \frac{\partial \omega_r^2}{\partial t_i}\mathbf{M} - \omega_r^2 \frac{\partial \mathbf{M}}{\partial t_i}\right)\boldsymbol{\varphi}_r + (\mathbf{K} - \omega_r^2 \mathbf{M})\frac{\partial \boldsymbol{\varphi}_r}{\partial t_i} = 0 \tag{11}$$

where ω_r and $\boldsymbol{\varphi}_r$ are the rth circular natural frequency and modal vector of the structure. Since the mass and stiffness matrices are a symmetric matrix, there exists

$$\boldsymbol{\varphi}_r^{\mathrm{T}}(\mathbf{K} - \omega_r^2 \mathbf{M}) = [(\mathbf{K} - \omega_r^2 \mathbf{M})\boldsymbol{\varphi}_r]^{\mathrm{T}} = 0 \tag{12}$$

Thus, pre-multiplying the vector $\boldsymbol{\varphi}_r^{\mathrm{T}}$ to Eq. (11) and considering Eq. (12) yield

$$\frac{\partial \omega_r^2}{\partial t_i} = \frac{\boldsymbol{\varphi}_r^{\mathrm{T}}\left(\frac{\partial \mathbf{K}}{\partial t_i} - \omega_r^2 \frac{\partial \mathbf{M}}{\partial t_i}\right)\boldsymbol{\varphi}_r}{\boldsymbol{\varphi}_r^{\mathrm{T}} \mathbf{M} \boldsymbol{\varphi}_r} \tag{13}$$

Eq. (13) can be rewritten in terms of natural frequency f_r in Hz

$$\frac{\partial f_r}{\partial t_i} = \frac{1}{8\pi^2 f_r} \cdot \frac{\boldsymbol{\varphi}_r^{\mathrm{T}}\left(\frac{\partial \mathbf{K}}{\partial t_i} - 4\pi^2 f_r^2 \frac{\partial \mathbf{M}}{\partial t_i}\right)\boldsymbol{\varphi}_r}{\boldsymbol{\varphi}_r^{\mathrm{T}} \mathbf{M} \boldsymbol{\varphi}_r} \tag{14}$$

Eq. (14) actually provides a way to calculate the sensitivity of the rth natural frequency to the change in thickness t_i of the ith structural member. Assuming that the steel space structure is linear and the change in natural frequency due to the reduction of member thickness is small, the change in the rth natural frequency, Δf_r, due to the reduction in thickness t_i of the ith structural member, Δt_i, can be expressed as

$$\Delta f_r = \frac{\partial f_r}{\partial t_i}\Delta t_i \tag{15}$$

It is seen that the determination of the sensitivity coefficient expressed by Eq. (14) depends on the determination of $\partial \mathbf{K}/\partial t_i$ and $\partial \mathbf{M}/\partial t_i$. This can be done based on the type of cross section of a structural member and the type of element used to model the structural member. For a truss element, the element stiffness matrix and element mass matrix are directly related to the cross section area, A, and the sensitivity of stiffness matrix and mass matrix to the change in thickness t_i of the ith element can be expressed as

$$\frac{\partial \mathbf{K}^e}{\partial t_i} = \frac{\partial \mathbf{K}^e}{\partial A_i} \cdot \frac{\partial A_i}{\partial t_i} \tag{16}$$

$$\frac{\partial \mathbf{M}^e}{\partial t_i} = \frac{\partial \mathbf{M}^e}{\partial A_i} \cdot \frac{\partial A_i}{\partial t_i} \tag{17}$$

For an Euler–Bernoulli beam element, the sensitivity of stiffness matrix and mass matrix to the change in thickness t_i of the ith element can be expressed as

$$\frac{\partial \mathbf{K}^e}{\partial t_i} = \frac{\partial \mathbf{K}^e}{\partial A_i} \cdot \frac{\partial A_i}{\partial t_i} + \frac{\partial \mathbf{K}^e}{\partial I_x} \cdot \frac{\partial I_{xi}}{\partial t_i} + \frac{\partial \mathbf{K}^e}{\partial I_y} \cdot \frac{\partial I_{yi}}{\partial t_i} + \frac{\partial \mathbf{K}^e}{\partial I_z} \cdot \frac{\partial I_{zi}}{\partial t_i} \tag{18}$$

$$\frac{\partial \mathbf{M}^e}{\partial t_i} = \frac{\partial \mathbf{M}^e}{\partial A_i} \cdot \frac{\partial A_i}{\partial t_i} + \frac{\partial \mathbf{M}^e}{\partial I_x} \cdot \frac{\partial I_{xi}}{\partial t_i} + \frac{\partial \mathbf{M}^e}{\partial I_y} \cdot \frac{\partial I_{yi}}{\partial t_i} + \frac{\partial \mathbf{M}^e}{\partial I_z} \cdot \frac{\partial I_{zi}}{\partial t_i} \tag{19}$$

in which I_{xi}, I_{yi}, I_{zi} are the second moment of inertia with respect to the local coordinates x, y, and z, respectively, of the ith structural member. In Eqs. (16)–(19), the first derivative of either the element stiffness matrix or the element mass matrix to the cross section area and one of the three second moments can be easily determined based on the conventional element stiffness and mass matrices available. For the typical cross section of a structural member, the first derivative of the cross section area and second moment to the change in thickness can also be determined. For instance, by omitting the second order and above of the change in thickness Δt, the aforementioned first derivatives to the thickness change caused by the reduction of inner surface of the circular cross section member can be derived as

$$\frac{\partial A}{\partial t^{\text{in}}} = 2\pi r_i \tag{20}$$

$$\frac{\partial I_y}{\partial t^{\text{in}}} = \frac{\partial I_z}{\partial t^{\text{in}}} = \pi r_i^3 \tag{21}$$

$$\frac{\partial I_x}{\partial t^{\text{in}}} = 2\pi r_i^3 \tag{22}$$

in which r_i is the inner radius of circular cross section of the structural member (see Fig. 1(a)). The first derivatives to the thickness change caused by the reduction of outer surface of the circular cross section member can be given as

$$\frac{\partial A}{\partial t^{\text{ou}}} = 2\pi r_o \tag{23}$$

$$\frac{\partial I_y}{\partial t^{\text{ou}}} = \frac{\partial I_z}{\partial t^{\text{ou}}} = \pi r_o^3 \tag{24}$$

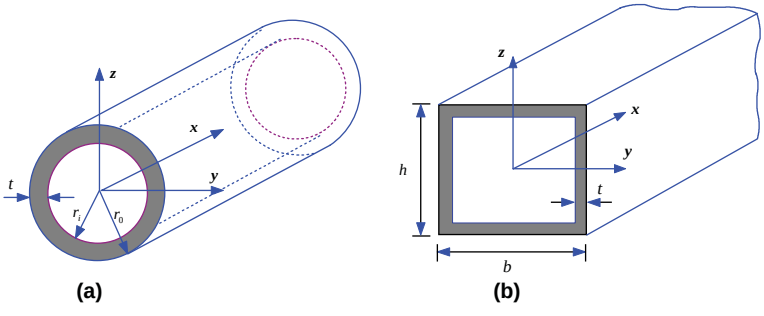

Fig. 1. Cross sections of typical structural members used in steel space structure: (a) circular section; (b) rectangular section.

$$\frac{\partial I_x}{\partial t^{\mathrm{ou}}} = 2\pi r_o^3 \tag{25}$$

in which r_o is the outer radius of circular cross section of the structural member. For the rectangular cross section member as shown in Fig. 1(b), the sensitivity coefficients with respect to the loss of thickness on the inner surface are

$$\frac{\partial A}{\partial t^{\mathrm{in}}} = 2b + 2h - 8t \tag{26}$$

$$\frac{\partial I_x}{\partial t^{\mathrm{in}}} = \frac{1}{6}(b + h - 4t)^3 \tag{27}$$

$$\frac{\partial I_y}{\partial t^{\mathrm{in}}} = \frac{(h - 2t)^2}{6}(3b + h - 8t) \tag{28}$$

$$\frac{\partial I_z}{\partial t^{\mathrm{in}}} = \frac{(b - 2t)^2}{6}(3h + b - 8t) \tag{29}$$

The sensitivity coefficients with respect to the loss of thickness on the outer surface of the structural member are

$$\frac{\partial A}{\partial t^{\mathrm{ou}}} = 2b + 2h \tag{30}$$

$$\frac{\partial I_x}{\partial t^{\mathrm{ou}}} = \frac{1}{6}(b + h)^3 \tag{31}$$

$$\frac{\partial I_y}{\partial t^{\mathrm{ou}}} = \frac{h^2}{6}(3b + h) \tag{32}$$

$$\frac{\partial I_z}{\partial t^{\mathrm{ou}}} = \frac{b^2}{6}(3h + b) \tag{33}$$

Once all the sensitivity coefficients of the element stiffness and mass matrices with respect to the thickness change are available, the assembly of them in accordance with the conventional finite element method yields the required matrices $\partial\mathbf{K}/\partial t_i$ and $\partial\mathbf{M}/\partial t_i$, by which the change in the rth natural frequency, Δf_r, due to the reduction in thickness t_i of the ith structural member, Δt_i, can be determined according to Eq. (15).

4. Stress changes due to atmospheric corrosion

The reduction of cross section thickness of all the structural members in a steel space structure due to atmospheric corrosion will cause stress changes, which will in turn affect the safety of the structure. In consideration that a large steel space structure may experience large deformation, a nonlinear static analysis is conducted in this study to assess the stress changes of the structure under gravity forces. Different from a linear static analysis, the nonlinear static analysis is based on the deformed structure, and the deformation and stress distribution of the structure in the final stage can only be determined through numerical iterations. The Newton–Raphson iteration method is thus used in this study, which makes the solution converge at each load increment to ensure the accuracy of the final computed results. The flow chart for the nonlinear static analysis of a large steel space structure due to atmospheric corrosion under gravity forces is shown in Fig. 2. The environmental parameters for the location where the

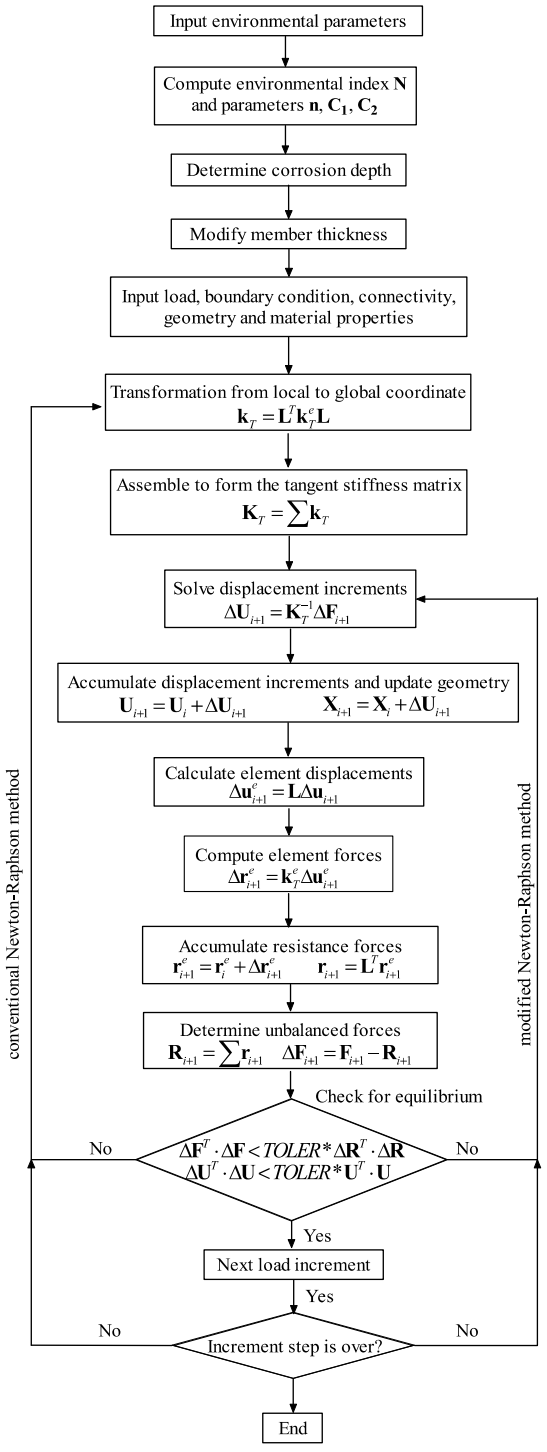

Fig. 2. Procedure of nonlinear static analysis for steel space structure subjected to atmospheric corrosion.

structure is built should be input first, from which the environmental index and other parameters in Eq. (7) can be estimated. The reduction of thickness of each member of the structure can then be calculated and input to compute the actual stiffness of the structural members. Finally, a standard nonlinear static analysis should be conducted. In Fig. 2, $\mathbf{k}_T$ and $\mathbf{k}_T^e$ are the tangent stiffness matrix of an element in the global and local coordinate, respectively. The matrix $\mathbf{K}_T$ is the total tangent stiffness matrix of the structure. $\mathbf{X}$, $\mathbf{U}$, and $\Delta\mathbf{U}$ are the nodal coordinate vector, displacement vector, and displacement increment vector, respectively, in the global coordinate. $\mathbf{u}$ and $\Delta\mathbf{u}$ are the displacement vector and displacement increment vector, respectively, in the local coordinate. $\mathbf{r}^e$ and $\Delta\mathbf{r}^e$ are the element force vector and element force increment vector, respectively, in the local coordinate. $\mathbf{r}$ and $\mathbf{R}$ are the element force vector and total internal force vector, respectively, in the global coordinate. $\mathbf{F}$ is the external force vector, and $\Delta\mathbf{F}$ is the unbalanced force vector. $\mathbf{L}$ is the transformation matrix from the global coordinate to the local coordinate for an element.

5. Case study

5.1. Description of a large steel space structure

Fig. 3 shows the elevation of a large steel space structure used to connect four buildings and provide roof function in order to form a well-integrated office complex as required by architects. The office complex is located in Shenzhen, a southern coastal city of China next to Hong Kong. The length of the steel space structure is 258 m in the east–west direction, and its width in the north–south direction varies from 130 m at the two ends to 120 m at the middle of the structure (see Fig. 4). The space structure possesses a curved elevation with the lowest level about 36 m above the ground at the two ends and the highest level about 73 m above the ground at the middle. The thickness of the space structure in the elevation varies from 4.47 m at the two ends to 8.79 m at the middle. The space structure is constructed with a triple-layer grid. The top layer, the middle layer, and the bottom layer of the space structure are formed as a square grid as shown in Fig. 5(a), (c), and (e), respectively, with two openings left for the connections with the circular tower and the rectangular tower through two huge truss girders. The top layer and the bottom layer are connected to the middle layer through the top brace system shown in Fig. 5(b) and the bottom brace system shown in Fig. 5(d) with all spherical joints welded. The two huge truss girders, as shown in Fig. 5(f), are connected to the triple-layer grid at the locations of the circular tower and the rectangular tower to form a complete space structure. One truss girder then sits on the circular tower through eight spherical bearings that are movable in all directions, and the other truss girder sits on the rectangular tower through four spherical bearings, as shown in Fig. 4. The space structure also sits on the east building and the west building at its two ends with a total of eight supports, each of which is formed using 16 members arranged in shape of a tree and connected to a spherical bearing, as shown in Figs. 4 and 5(g).

A three-dimensional finite element model is established for the steel space structure using a commercial computer package. The model has a total of 12,499 beam elements and 2921 nodes with 6 degrees of freedom at each node. All the joints in the finite element model are assumed to be rigid. Each spherical bearing is modeled as two springs arranged in the x- and y- direction respectively. The movement of all the supports in the vertical direction is restricted. For the sake of convenience in the subsequent discussion, the beam elements in each component of the steel space structure are numbered differently. The beam elements in the eight tree-shaped supports are numbered from 1 to 128 (denote zcg), the elements in the bottom layer are numbered from 129 to 2086 (denote xxg), the elements in the bottom brace system are counted from 2087 to 5315 (denote xfg), the elements in the middle layer are counted from 5316 to 6938 (denote zxg), the elements in the top brace system are counted from 6939 to 10,180 (denote sfg), the elements in the

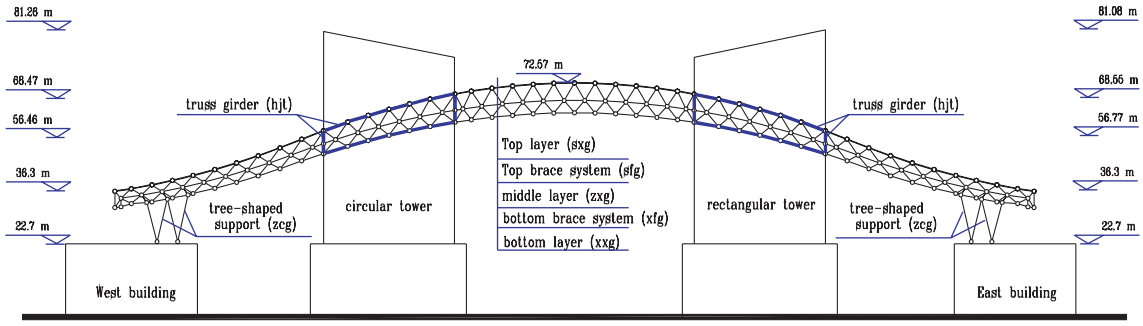

Fig. 3. Elevation of a large steel space structure.

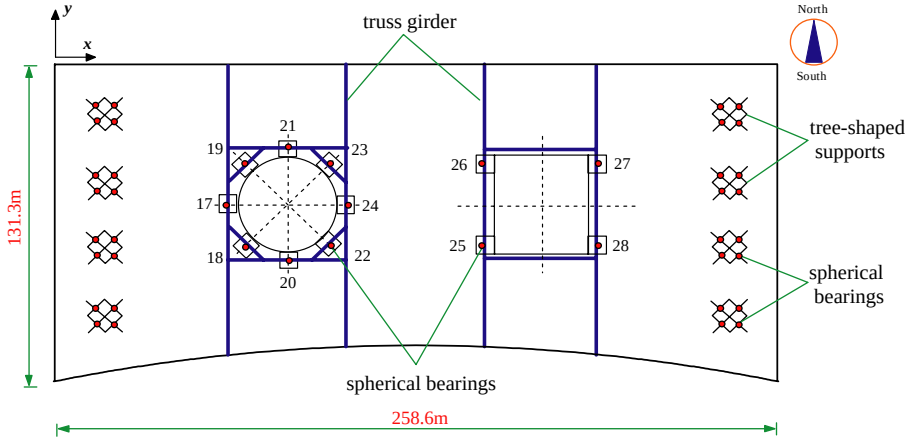

Fig. 4. Plane view of a large steel space structure.

top layer are counted from 10,181 to 11,810 (denote sxg), and the elements in the two truss girders are counted from 11,811 to 12,499 (denote hjt). The number of elements in the eight three-shaped supports is only 1% of the total number of elements used in the structure while the number of elements in the two truss girders is 5.5% of the total number of elements used in the structure. The structural members used in the eight three-shaped supports and the two truss girders are made of Q345A steel (16Mn) with a yielding stress of 345 MPa. The structural members used in the three layers and the two brace systems are made of Q235B steel (A3) of a yielding stress of 235 MPa. Except that the main chords in the two truss girders are of hollow rectangular section, all the other members are of hollow circular section.

5.2. Dynamic characteristics and stress levels of the structure without corrosion

The dynamic characteristics analysis is conducted based on the established finite element model of the steel space structure. The first 10 vibration modes of the structure are depicted in Fig. 6. The first vibration mode is a global vibration mode mainly due to the movement of spring supports in the y-direction. The second vibration mode is also a global vibration mode but mainly due to the movement of spring supports in the x-direction. The third vibration mode is a global torsional vibration mode in the x–y plane due to the

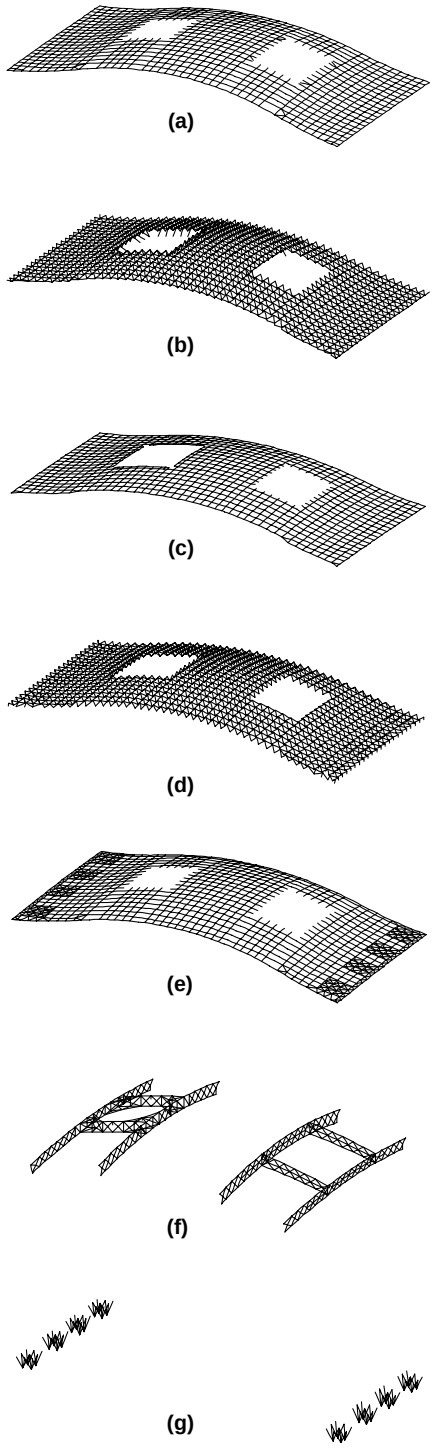

Fig. 5. Structural components: (a) top layer (sxg); (b) top brace system (sfg); (c) middle layer (zxg); (d) bottom brace system (xfg); (e) bottom layer (xxg); (f) truss girders (hjt); (g) tree-shaped supports (zcg).

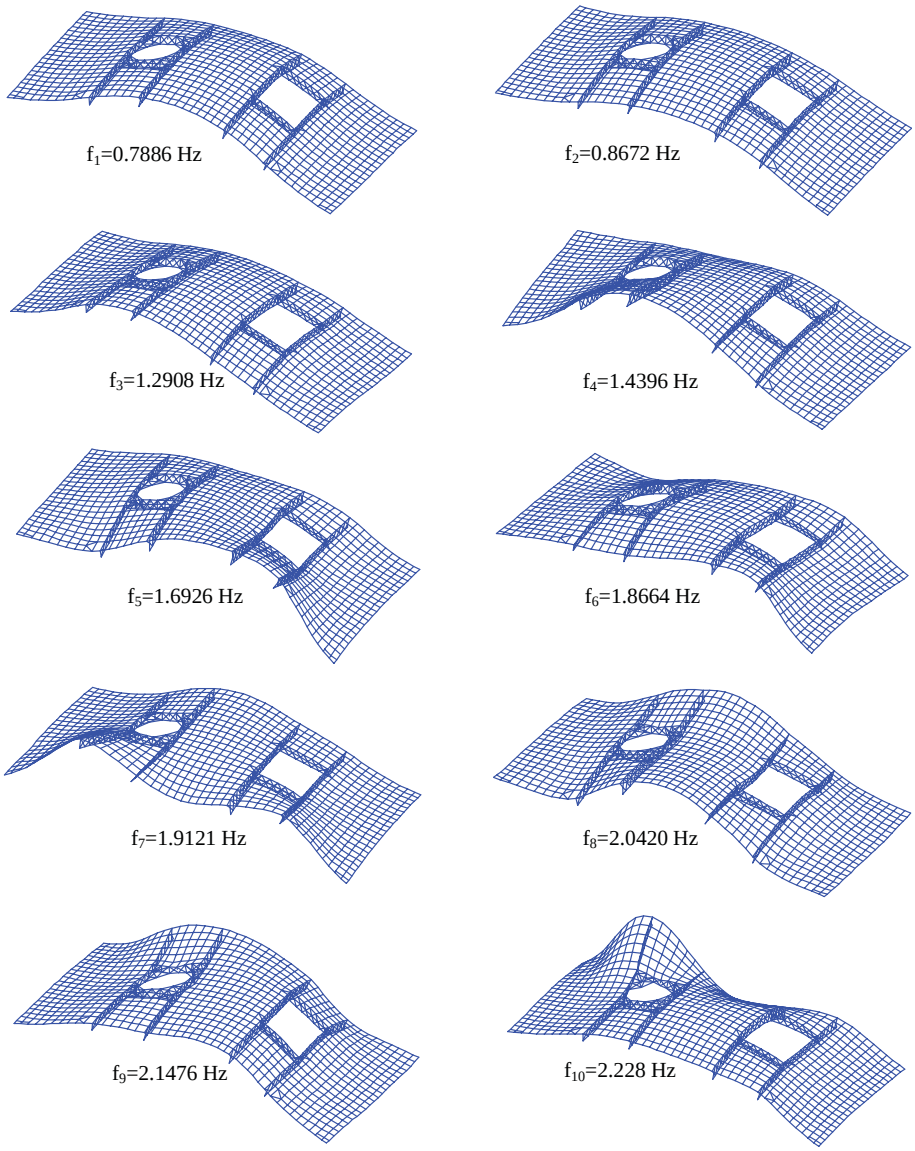

Fig. 6. The first 10 natural frequencies and mode shapes of the structure.

movement of spring supports. The fourth to 10th vibration modes all appear mainly in the vertical direction because of the movements of the two truss girders in different combinations. The first 10 natural frequencies computed indicate that the natural frequencies of the structure are closely spaced. The field measurement of vibration modes of the structure may be a difficult task.

The nonlinear static analysis of the space structure under dead loads is also executed to find stress levels of all the structural members. Fig. 7 shows the percent ratio of working stress to yielding stress of all the structural members. The maximum stress level is less than 80%. The number of structural members with the stress ratio less than 10% accounts for 73% of the total structural members, and the 99.5% structural mem-

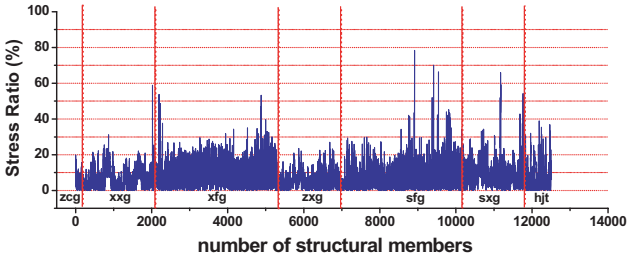

Fig. 7. Ratio of working stress to yield stress of all the structural members.

bers have a stress ratio less than 30%. Only two members have a stress level between 70% and 80%. In general, the structural members in the two truss girders and the two brace systems have higher stress level than those in the eight tree-shaped supports and the three layers. It is noted that the stress levels calculated here consider dead loads only. Wind loads are not included in the calculation but will be considered in a later stage.

5.3. Atmospheric corrosion of materials

The empirical model presented in Section 2 is now applied to predict the atmospheric corrosion depth of the steel members of the space structure. Fig. 8 shows the relative locations of Shenzhen and other seven cities. The national experimental network has obtained the environmental index N and the atmospheric corrosion trend n for the seven cities but not for Shenzhen. Therefore, the environmental parameters of Shenzhen are collected and listed in Table 1. The environmental index N of Shenzhen is calculated as 1.113 using Eq. (3). This value is similar to that of Guangzhou and Wanning. To determine the atmospheric corrosion trend n for Shenzhen, the pattern recognition technique expressed by Eqs. (8) and (9) is used. The seven matching degrees are depicted in Fig. 9 for the seven cities. The best match to Shenzhen is Guangzhou, which is a city nearest to Shenzhen (see Fig. 8). Both cities are affected by industrial atmosphere, and the contamination contents in Shenzhen are close to Guangzhou. Thus, it is reasonable to use the coefficient n of Guangzhou for Shenzhen, that is, $n = 0.48$ for Q345A steel and $n = 0.45$ for Q235B steel according to Table 2. The constants C_1 and C_2 are 39.55 and 65.94 for Q345A steel, and 39.36 and 61.34 for Q235B steel according to Table 3.

With all the model parameters determined, the corrosion depth of steel members in the space structure can be predicted using Eq. (7). Fig. 10 shows the variation of corrosion depth of Q235B steel and Q345A steel with time in year. Fig. 11 displays the variation of corrosion rate with time in year. It is seen that the corrosion depth of the two materials increases with time. Q235B steel has relatively smaller corrosion depth than Q345A steel. The atmospheric corrosion rate of the material depth is almost the same for the two materials. It is clear that the corrosion rate of material depth is much faster in the first 5 years than later.

5.4. Effects of atmospheric corrosion on natural frequencies

The steel space structure concerned is made of steel members of either circular or rectangular hollow section. The outer surfaces of all the structural members are painted to prevent atmospheric corrosion, but the inner surfaces of all the structural members are not painted because of operation inconvenience. To this end, the atmospheric corrosion on the inner surfaces of the structural members should be considered. Nevertheless, the atmospheric corrosion on both the inner and outer surfaces is also considered as an

Fig. 8. Location of Shenzhen and other 7 cities in China.

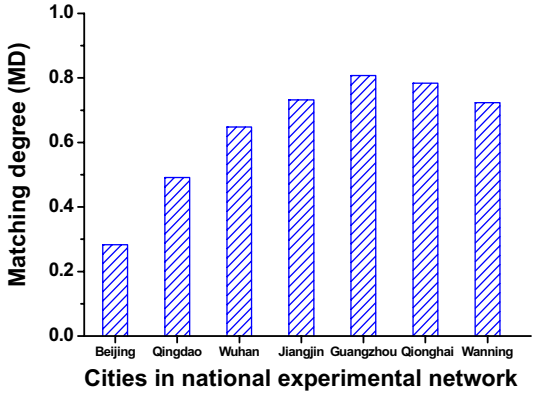

Fig. 9. Matching degree of Shenzhen to other 7 cities.

extreme case and compared with the case of inner surface corrosion only. For either case, the sensitivity of the rth natural frequency to the change in thickness t_i of the ith structural member is first computed using Eq. (14). The change in the rth natural frequency, Δf_r, due to the reduction in thickness t_i of the ith structural member, Δt_i, is then computed using Eq. (15). Finally, the algebraic summation of the changes in the rth natural frequency due to the reductions in thickness of all the structural members gives the final change

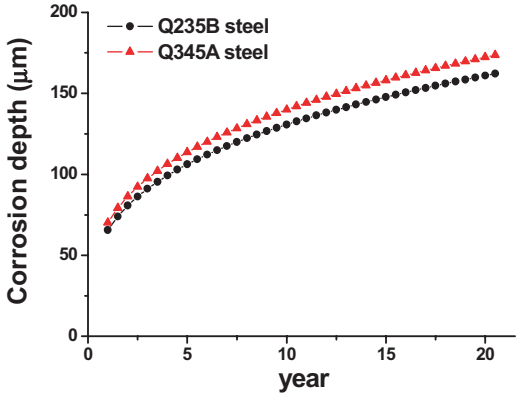

Fig. 10. Variation of corrosion depth of materials with time.

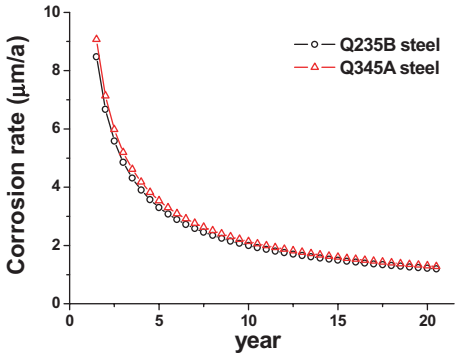

Fig. 11. Variation of corrosion rate of materials with time.

in the rth natural frequency, from which the effect of atmospheric corrosion on the rth natural frequency can be assessed.

Fig. 12 shows the sensitivities of the first 10 natural frequencies to the thickness change of each member due to inner surface corrosion. It is seen that the first three natural frequencies are more sensitive to the thickness change of members in the eight tree-shaped supports than structural units. All the higher natural frequencies are more sensitive to the thickness change of members in the two truss girders than other structural units. This is consistent with the structural configuration and the modes of vibration: the first three modes of vibration are mainly due to the movement of the supports while the higher modes of vibration are mainly due to the movement of the two truss girders. It is noted that the first and sixth natural frequencies are also sensitive to the thickness change of some of members in the two brace systems. However, the thickness changes of structural members in the middle layer of the structure due to corrosion affect the natural frequencies only slightly despite their important connection functions between the top and bottom layers.

The changes in natural frequencies of the structure due to inner surface corrosion are displayed in Fig. 13 for the corrosion period of 1, 4, 10 and 20 years, respectively. The changes in the first 5 natural frequencies with corrosion time are shown in Fig. 14. It is seen that as corrosion years increase, the changes in natural

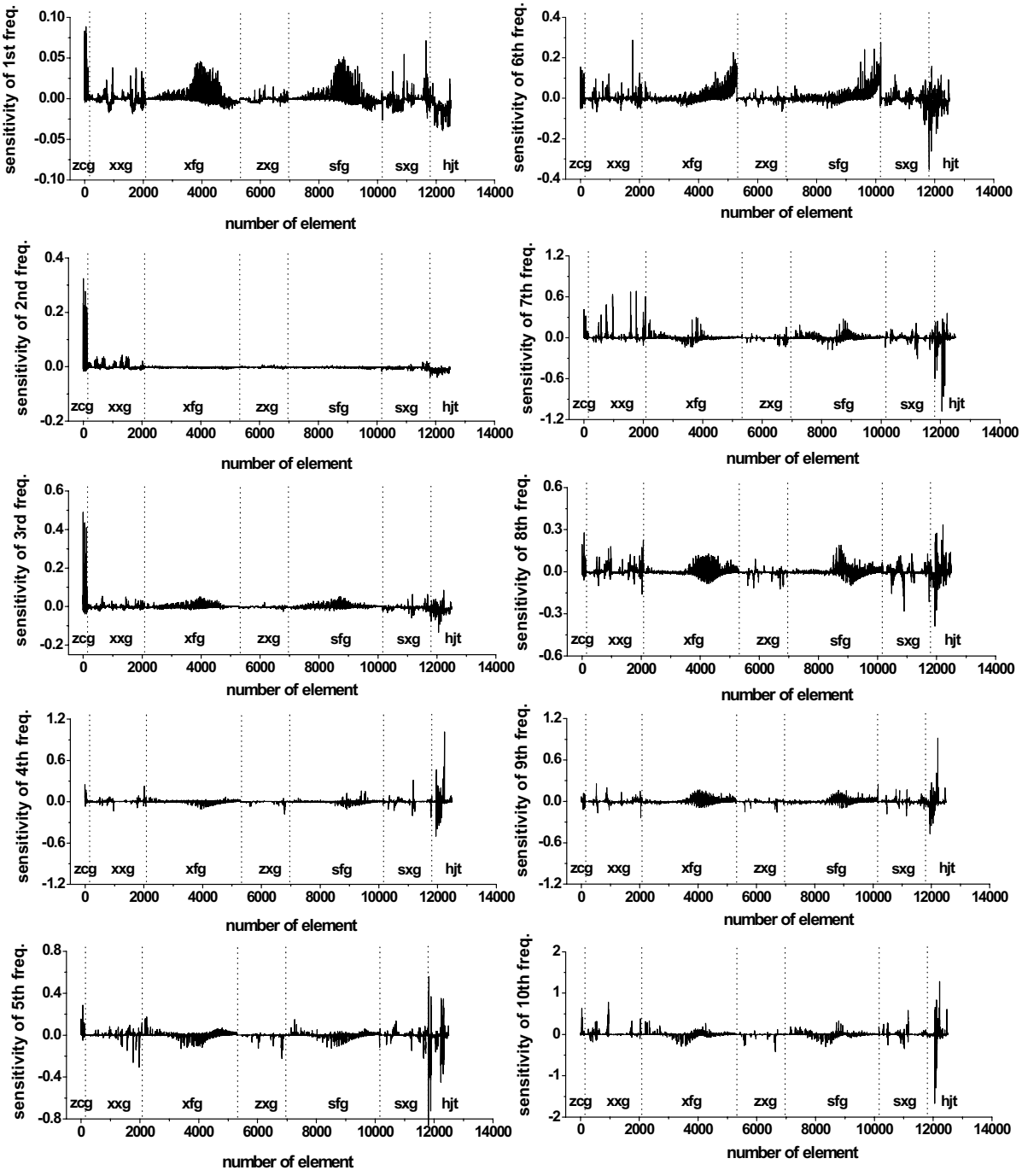

Fig. 12. Sensitivity of first 10 natural frequency to thickness change of all the structural members (inner surface corrosion).

frequencies also increase. The changes in the first 5 natural frequencies are negative, indicating that the natural frequencies are reduced. The second natural frequency of the structure has the maximum change

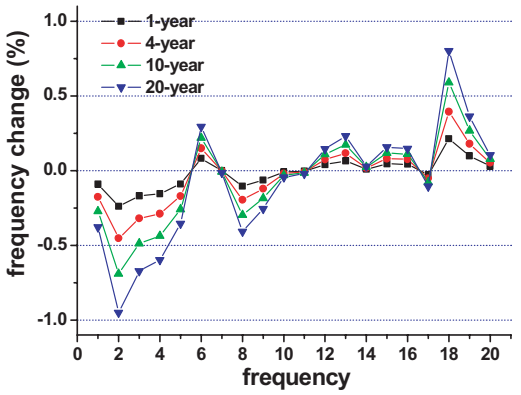

Fig. 13. Frequency changes for different corrosion periods.

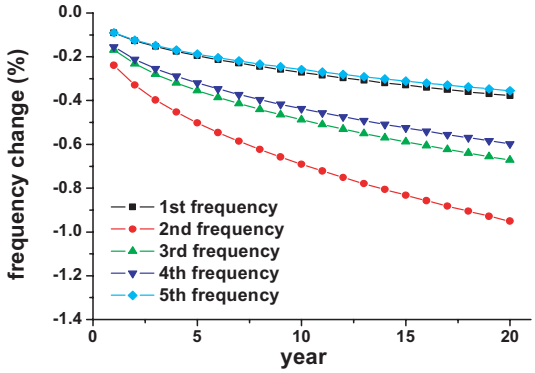

Fig. 14. Variation of the first 5 natural frequency with time.

due to inner surface corrosion. The changes in some of higher natural frequencies are positive, implying that these natural frequencies are actually increased. This is because while the reduction of member thickness due to corrosion causes the stiffness reduction, it also causes the mass reduction. Whether the change in a natural frequency is positive or negative depends on the relative extent of the stiffness reduction effects and the mass reduction effect.

It is seen that the second natural frequency of the structure has the maximum change due to inner surface corrosion. The maximum change in the second natural frequency due to inner surface corrosion is about 1% in 20 years. Even though both the inner and outer surface corrosions are considered, the maximum change in the second natural frequency is about 2% in 20 years. Therefore, it can be concluded that the natural frequencies of the large steel space structure considered in this study are only slightly affected by the atmospheric corrosion of materials. However, this conclusion may not be applicable to other steel space structures in other places.

5.5. *Effects of atmospheric corrosion on member stresses*

The effects of atmospheric corrosion on member stresses of the structure under gravity forces are investigated in this section. The atmospheric corrosion will cause the reduction of cross section areas of the

structural members, and therefore it will also cause the reduction of gravity forces and structural stiffness. Such changes will in turn affect the level and distribution of structural member stresses. On the other hand, the gravity forces of other structural components, such as joints and cladding, are regarded as constant forces acting on the structural nodes without changes. Nonlinear static analyses of the structure are then carried out according to the computation algorithm shown in Fig. 2 for 10-, 20-, and 50-year atmospheric corrosion.

Fig. 15 shows the statistics of structural members with various levels of stress change under 10-, 20- and 50-year atmospheric corrosion. The results shown in Fig. 15(a) are for inner corrosion only while the results displayed in Fig. 15(b) are for double surface corrosion. It is seen from Fig. 15(a) that

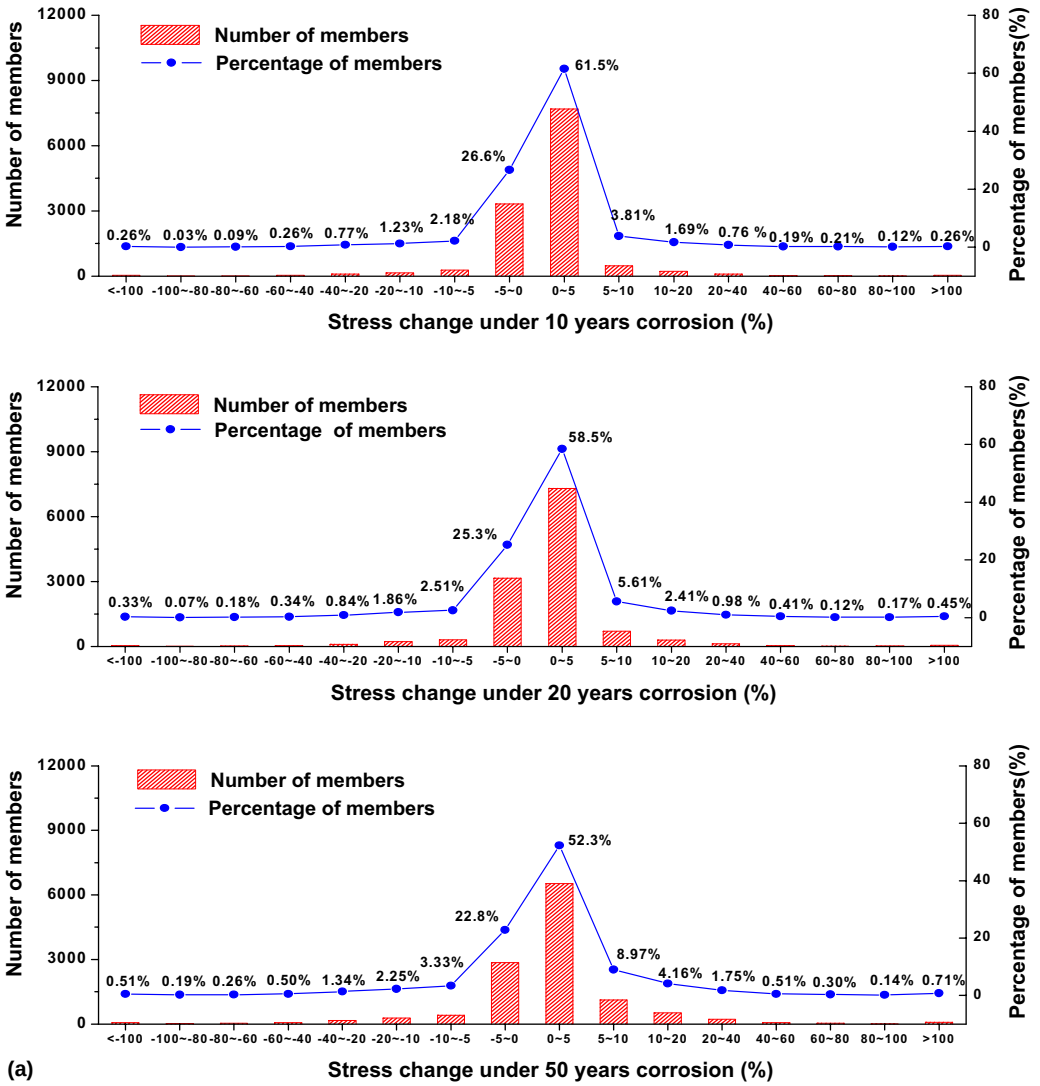

Fig. 15. Statistics of structural members with various levels of stress change (a) corrosion on inner surface; (b) corrosion on both surfaces.

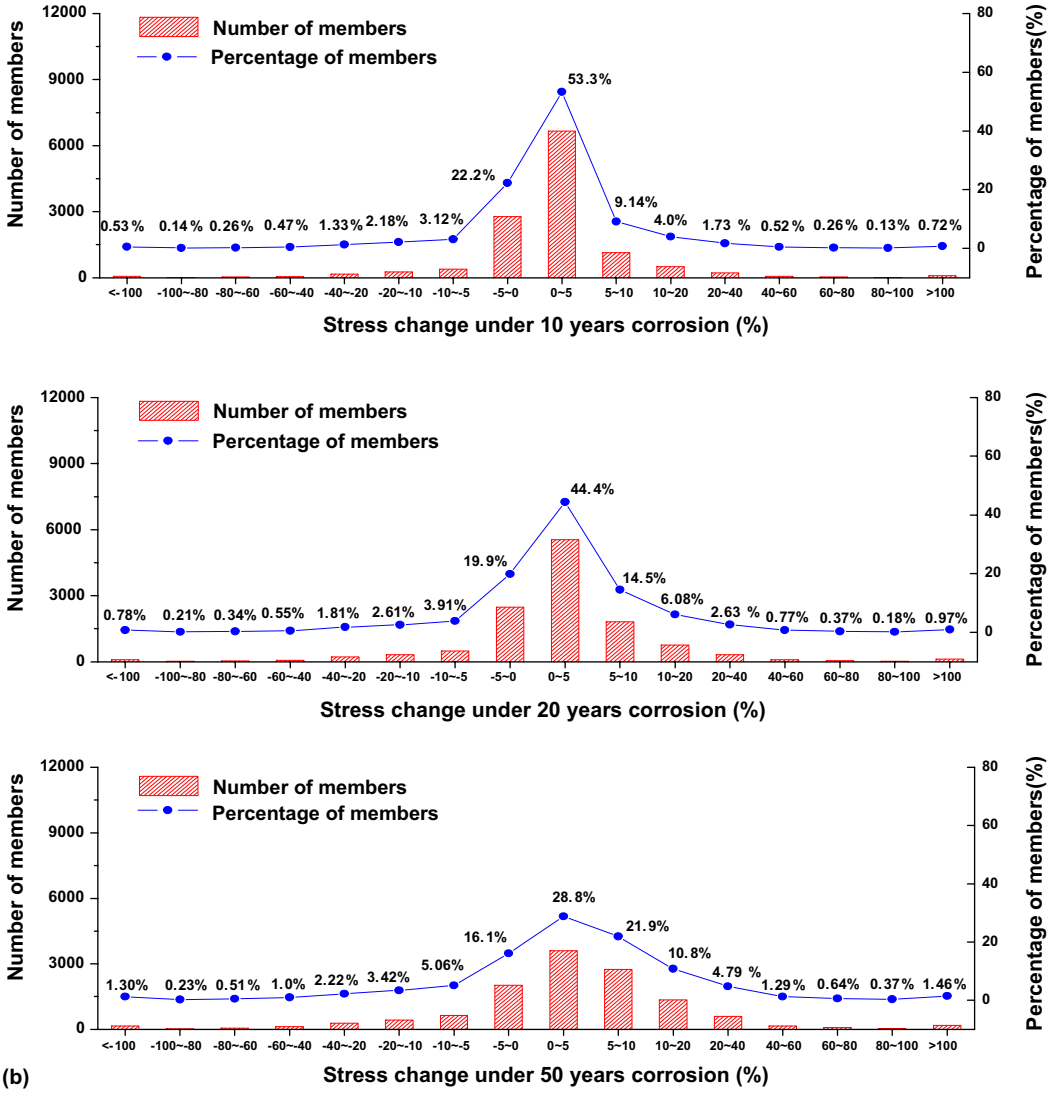

Fig. 15 (*continued*)

94.1%, 91.9% and 87.4% of the structural members have a stress change no more than ±10% for 10-, 20- and 50-year atmospheric corrosion, respectively. The structural members having a stress change large than ±100% are 0.52%, 0.78% and 1.21% of the total structural members for 10-, 20-, and 50-year atmospheric corrosion, respectively. It is clear that with the increase of atmospheric corrosion year, the numbers of structural members with large stress change increase. There exist both negative and positive stress changes, indicating stress redistribution in the structure. Nevertheless, the structural members of increasing stress are more than those of decreasing stress. Similar observations can be made for the structural members with double surface corrosion, as shown in Fig. 15(b). Compared with the structural members of inner surface corrosion only, the numbers of structural members of large stress change significantly

increase while the numbers of structural members of small stress change considerably decrease when double surface corrosion is considered.

To further illustrate the stress change and redistribution, the stress changes in 128 structural members of the eight tree-shaped supports are plotted in Fig. 16(a) for inner surface corrosion only and Fig. 16(b) for double surface corrosion. It is seen that though the stresses in most of the structural members are only slightly affected by atmospheric corrosion, a few of structural members have large stress change and such a stress change increases with increasing corrosion year. For a 50-year atmospheric corrosion, the maximum stress change reaches 93% for inner surface corrosion and it reaches about 200% for double surface corrosion. Though the stress changes in the structural members due to double surface corrosion are much larger than those due to inner surface corrosion, the structural members of large stress changes remain almost in the same positions.

A careful examination of stress changes in all the structural members reveals that for the concerned structure, the structural members of higher stress level have small stress change only while large stress changes occur in the structural members of lower stress level. Listed in Table 4 are the stress changes in the two structural members of the highest stress level due to inner surface corrosion. The two members belong to the top brace system. It is seen that the stress change increases with increasing corrosion year but the stress change is small and less than 4% even with a 50-year corrosion year. However, such results may not be applicable to other structures in other places.

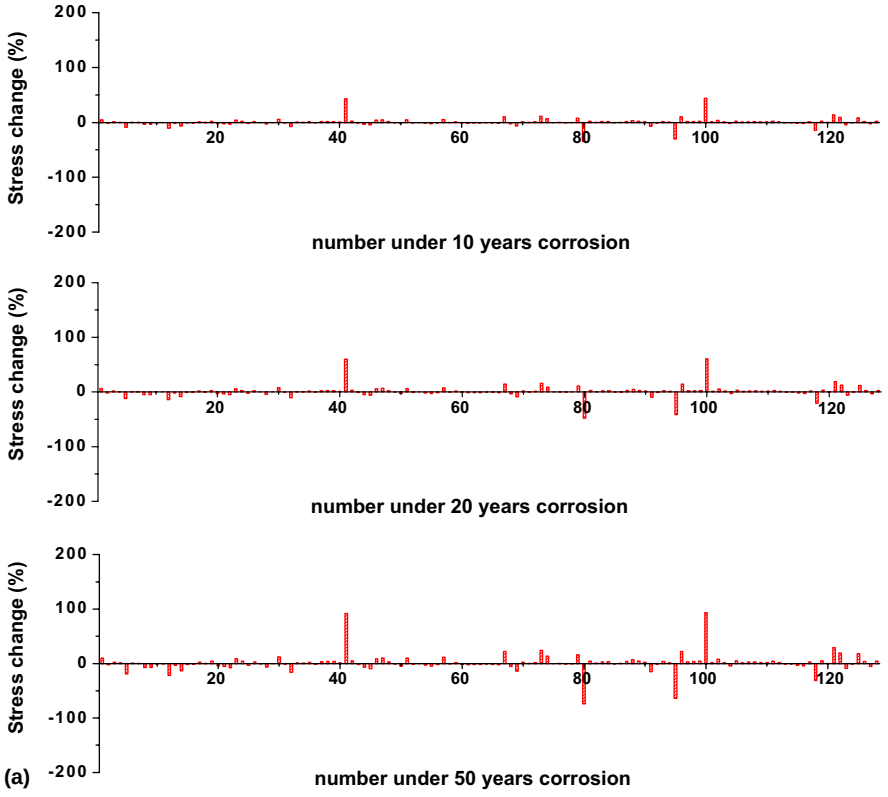

Fig. 16. Stress change in eight tree-shaped supports: (a) corrosion on inner surface; (b) corrosion on both surfaces.

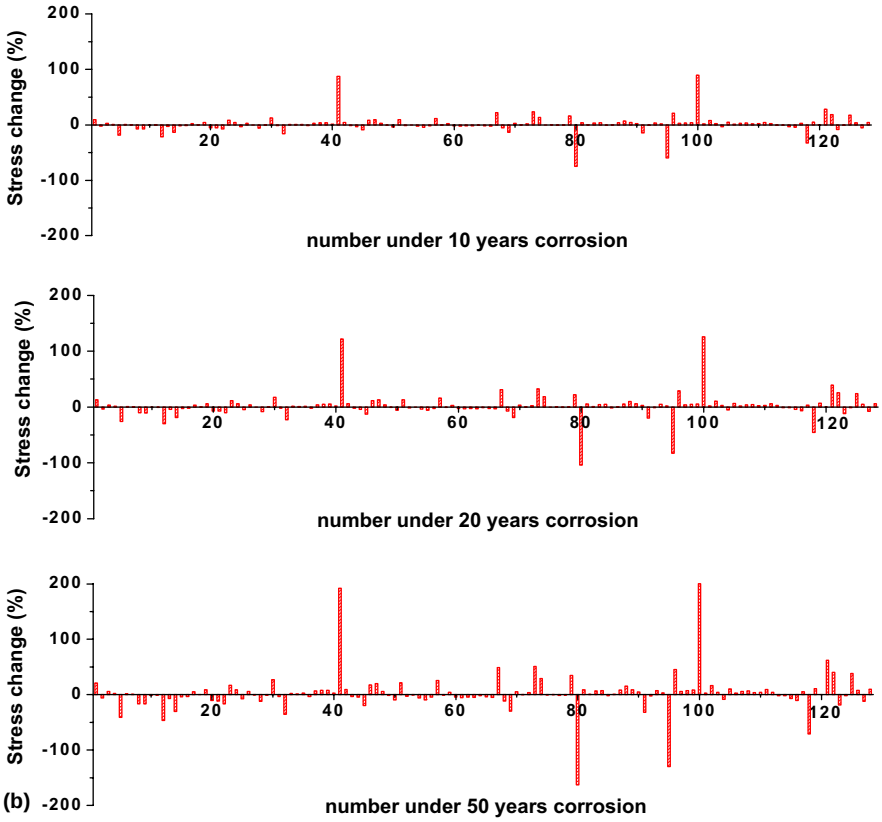

Fig. 16 (*continued*)

Table 4
Stress changes in the two structural members of the highest stress level due to inner surface corrosion

Element		No corrosion	4-year corrosion	10-year corrosion	20-year corrosion	50-year corrosion
8911	Stress level (%)	78.3	79.3	79.8	80.3	81.4
	Stress change (%)	0	1.0	1.5	2.0	3.1
9412	Stress level (%)	70.0	70.7	71.1	71.5	72.3
	Stress change (%)	0	0.7	1.1	1.5	2.3

6. Concluding remarks

A framework for evaluation of potential damage due to atmospheric corrosion to steel space structures in coastal areas has been established and applied to a real large steel space structure built in southern coastal area in China. The case study demonstrates the feasibility of the proposed framework. The case study also shows that the changes in natural frequencies of the steel space structure due to either inner surface corrosion or double surface corrosion are very small but the stress changes in some of structural members are very large. The stress changes increase with increasing atmospheric corrosion year, and they are

larger in the case of double surface corrosion than in the case of inner surface corrosion only. Fortunately, for the concerned structure the structural members of higher stress level have smaller stress change.

It is worthwhile to point out that the results obtained from the structure concerned may not be applicable to other structures in other places. The framework proposed here can be used to perform assessment case by case. Moreover, apart from atmospheric corrosion other corrosions such as stress corrosion deserve further investigation.

References

Batis, G., Rakanta, E., 2004. Corrosion of steel reinforcement due to atmospheric pollution. Cement & Concrete, 1–7.

Christofer, L., Thomas, T.G. et al., 2000. Atmospheric Corrosion. John Wiley.

Cole, L.S., 1994. Recent progress in modeling atmospheric corrosion. In: Proceeding of the 11th Asian-Pacific Corrosion Control Conference. Hochiminh City, Viemam, p. 94.

Cowell, D., Apsimon, H., 1996. Estimating the cost of damage to buildings by acidifying atmospheric pollution in Europe. Atmospheric Environment 30, 2959–2968.

Farrow, L.A., Graedel, T.E., 1996. Glides model studies of aqueous chemistry: II—The corrosion of zinc in gaseous exposure chambers. Corrosion Science 38, 2181.

Feliu, S., Morcillo, M., 1993a. The prediction of atmospheric corrosion from meteorological and pollution parameters (I): Annual corrosion. Corrosion Science 34, 403–414.

Feliu, S., Morcillo, M., 1993b. The prediction of atmospheric corrosion from meteorological and pollution parameters (II): Long-term forecasts. Corrosion Science 34, 415–422.

Flavio, D., Stefano, R., 2002. Premature corrosion failure of structural highway components made from weathering steel. Engineering Failure Analysis 19, 541–551.

Fox, R.L., Kapoor, M.P., 1968. Rates of change of eigenvalues and eigenvectors. AIAA 6 (12), 2426–2429.

Herrera, J.M., Spencer, P.R. et al., 1995. A failure analysis case study: Structural steel sign post collapse. Materials Characterization 34, 57–61.

Hou, W.T., et al., 1994. Evaluation of atmospheric corrosion of 7 test sites in China and corrosion mechanism of steels. Journal of Chinese Society for Corrosion and Protection 6, 137–142 (in Chinese).

Hou, W.T., Liang, C.F., 2004. Atmospheric corrosion prediction of steels. Corrosion Science 60, 313–322.

Ibrahim, M.A., Mohammed, M. et al., 1994. Influence of atmospheric corrosion on the mechanical properties of reinforcing steel. Construction and Building Materials 8, 35–41.

Juan, J.S.R., et al., 2003. The effect of environmental and meteorological variables on atmospheric corrosion of carbon steel, copper, zinc and aluminum in a limited geographic zone with different types of environment. Corrosion Science 45, 799–815.

Kucera, A., et al., 1986. Influence of acid deposition on atmospheric corrosion of metals—a review. ACS Symposium Series, 104–118.

Liang, C.F., Hou, W.T., 1998. Atmospheric corrosion for steels. Journal of Chinese society for corrosion and protection 18, 1–6 (in Chinese).

Mottershead, J.E., Friswell, M.I., 1993. Model updating in structural dynamics: a survey. Journal of Sound and Vibration 167 (2), 347–375.

Ninomiya, S., Ono, T., Udagawa, S., et al., 1997. Study on the influence of acid deposition on cultural properties. In: Proceedings of International Conference on the Effects of Acid Deposition on Cultural Properties and Materials in East Asia, pp. 22–28.

Shastry, C.R., Friel, J.J., et al., 1988. Degradation of Metals in Atmosphere, ASTM STP965.

Shreir, L.L., et al., 1994. Corrosion: Volume 1 Metal/Environment Reactions. British Library Cataloguing in Publication Data.

Wang, X.Y., Wang, G.Y. et al., 1995. The effect of environmental factors on atmospheric corrosion of carbon and low alloy steels. Journal of Chinese Society for Corrosion and Protection 15, 124–128 (in Chinese).